Research Article

Yuan Gao, Hongwen Jing*, and Zefu Zhou

Fractal analysis of pore structures in graphene oxide-carbon nanotube based cementitious pastes under different ultrasonication

https://doi.org/10.1515/ntrev-2019-0010
Received Mar 18, 2019; accepted Apr 11, 2019

Abstract: Nano cement additive using a hybrid of graphene oxide (GO) and multi-walled carbon nanotubes (MWCNTs) combines the excellent affinity of GO and the superior mechanical properties of MWCNTs. Ultrasonication is the key process to disperse the GO/MWCNTs and further optimizes the pore structures of cement-based pastes. Fractal dimension can effectively and quantitatively characterize the pore structures of cementitious composites. The present study investigates the fractal dimensions of pore structures of GO/MWCNT-OPC pastes under power- and time-controlled ultrasonication based on the mercury intrusion porosimetry (MIP) tests data. The finding of this study shows that comparing to calculating the fractal dimension of the overall pore size range, assessing the variations of fractal dimension of individual pore size range is more effective in evaluating the pore characteristic. The fractal dimension of larger capillary pores ($D_{>10^4\ nm}$) can be use to describe the change of pore structure of GO/MWCNT-OPC pastes under ultrasonication treatment with sufficient accuracy as higher value of $D_{>10^4\ nm}$ indicates better pore characteristics. The fractal dimension change trend of mesopores is always opposite to that of bigger capillary pores. Modest increment in both power- and time-controlled ultrasonication seems to result in the increase of the fractal dimension of capillary pores and lead to better reinforcement effects. Prolongation of ultrasonication time slightly influences the pore structure of the specimens, while nano cement additives exposed to excess ultrasonication power fail to afford adequate reinforcing effect and finally cause the deterioration of the pore structures. The findings of this study can provide helpful information of GO/MWCNT-OPC pastes and ultrasonication treatment in the future.

Keywords: Graphene oxide, Multi-walled carbon nanotubes, Ultrasonication, Fractal dimension, Cement, Pore structures

1 Introduction

The pore characteristic is one of the key factors which significantly influence the mechanical properties [1, 2], permeability [3] as well as durability [4] of cementious material. Fractal theory has been widely used to characterize actual pore structure of porous materials since first introduced by Mandelbrot in 1979 [5]. After that researchers proposed various models and some well-known fractal patterns include Koch curve, Cantor bar, Sierpinski carpet and Mensor [6]. Although the pore structure of actual cement-based materials is much more complex than aforementioned fractal models, fractal dimension, in addition with other parameters such as intruded volume, average pore diameter and porosity, comprehensively considered the pore size distribution range and all of the above mentioned items is regard as a effective parameter for characterization of the microstructure [7].

Multiple methods are applied to characterize the pore structures of cement-based materials, including scanning electronic microscopy [8], mercury intrusion porosimetry (MIP) [9, 10], nuclear magnetic resonance [11] and small angle scattering of X-rays [12]. Among these techniques, MIP is the most common applied method due to its simple experimental procedure and the capability to capture various pore sizes ranging from nano- to milli-meter [13, 14].

Multi-walled carbon nanotubes (MWCNTs) have been utilized as nano-reinforcement to overcome the shortcomings of brittle cementitious materials [15, 16]. Graphene oxide (GO) as another outstanding cementitious composite additive, with several kinds of oxygen-containing func-

***Corresponding Author: Hongwen Jing:** State Key Laboratory for Geomechanics & Deep Underground Engineering, China University of Mining & Technology, Xuzhou, China; Email: hongwenjingcumt@126.com
Yuan Gao, Zefu Zhou: State Key Laboratory for Geomechanics & Deep Underground Engineering, China University of Mining & Technology, Xuzhou, China

tional groups, can both accelerate hydration reaction and densify the pore structure of cement pastes [17–20]. Using a hybrid of GO and MWCNTs as nano-reinforcement may be a better alternative. As this method can combine the affinity, well dispersibility of GO and the superior mechanical properties of MWCNTs. Zhang *et al.* [21] proposed that the interaction among GO sheets and MWCNTs involved π-π interactions, contributes to more stable disperse of MWCNTs in suspensions. Zhou *et al.* [22] reported that GO may act as the dispersant for MWCNTs to overcome agglomeration and showed the excellent reinforcing capabilities of their hybrid mixture in cementitious matrix. Gao *et al.* presented that mixing the multiple additives of GO/MWCNTs into cementitious composite may lead to an enhancing efficiency both in mechanical properties [15] and permeability [23].

Ultrasonication is frequently applied for the dispersion of GO and MWCNTs [24, 25]. The significance of picking a suitable ultrasonication energy that balances the separating effect and scissoring effect of the ultrasonication during the process has been widely emphasized in dispersion fabrication [26, 27]. However, there still lack of understandings on the influence of ultrasonication treatment on the GO/MWCNTs hybrid dispersion in cement-based materials, particularly the effect on the pore structure characteristics.

In this research, the fractal dimensions of pore structures in GO/MWCNT-OPC pastes under various ultrasonication treatments were systematically studied. A fractal model based on the Menger sponge pattern has been reviewed and the method of calculating fractal dimension of the cement-based pastes is then introduced. The pore size distribution data of the GO/MWCNT-OPC specimens was achieved through MIP tests. The results of this research reveal that it is more effective in characterizing the pore structures to assess the variations of fractal dimension of individual pore size range than overall section. The fractal dimension of larger capillary pores ($D_{>10^4\ nm}$) is most accurate in characterizing the pore structure. The moderate increment of ultrasonication energy reinforces the pore structures of GO/MWCNT-OPC pastes, while excess ultrasonication power causes the deterioration of the pore structures. The findings of this research combine fractal analysis with ultrasonication treatment in the process of fabrication of GO/MWCNT-OPC pastes, and provide a new method to analyze ultrasonication effect from the fractal dimension of materials pore structures.

2 Fractal models

During recent years, fractal theory has provided a particularly quantitative framework to describe the cement-based materials physical phenomena over a range of temporal and spatial scales [6, 28]. The established model of Menger sponge algorithm has been used to simulate the intergranular pore structures of cementitious composites [29]. The process of the construction of typical Menger sponge model mainly consists of four stages as follows: first, a cube with unit length was subdivided into m^3 smaller cubes of equal size. Then, n cubes are removed from the m^3 cubes to leave (m^3-n) cubes based on a specific rule. Furthermore, repeating the above two steps, the amounts of remained cubes are growing while the corresponding cube size is reduced. After repeating k times, the overall cube number N_k is $(m^3\text{-}n)^k$ and the side length r_k of the remained small cubes is $1/m^k$. The remained smaller cubes form the three-dimensional skeleton, with the volume V_k, and the removed cubes form the pore structures whose volume is marked as V_P. According to the fractal theory, the relations between N_k and r_k can be described as:

$$N_k = {r_k}^{-D_M} \tag{1}$$

Where D_M represents the fractal dimension of the pore volume, is obtained as:

$$D_M = \lg(m^3 - n)/\lg m \tag{2}$$

Then, multiplying the volume ${r_k}^3$ of the small cube after iterations of k times on the both sides of the Eq. (1) to obtain

$$V_k \propto r_k^{3-D_M} \tag{3}$$

According to a cube of unit length, the volume is linked to two items, *i.e.*, pore volume V_P, and matrix volume V_k, with the relation of $V_P + V_k = 1$. Therefore, taking derivation on both sides of the Eq. (1) to obtain

$$-\frac{dV_p}{dr} \propto r^{2-D_M} \tag{4}$$

Then, taking the logarithm of the Eq. (4) yields the following equation:

$$\lg(-\frac{dV_p}{dr}) \propto (2 - D_M)\lg r \tag{5}$$

During the MIP test, a fixed input pressure of $P(r)$ is demanded to inject mercury into a certain pore size with the diameter of r. The relation between the pore size and cumulative pressure can be written using the Washburn method as [30]:

$$P(r) = (-4\gamma\cos\theta)/r \times 100\% \tag{6}$$

Table 1: Chemical composition of OPC (%).

CaO	SiO_2	Al_2O_3	Fe_2O_3	SO_3	MgO	K_2O	TiO_2	Others	Loss
65.01	20.69	5.71	4.18	2.52	0.61	0.61	0.31	0.32	3.26

Table 2: Physical properties of MWCNTs.

Outer diameter	Inner diameter	Length	Purity	Specific Surface Area	Tap density	True density
> 50 nm	5–15 nm	10–20 μm	> 95%	> 40 m^2/g	0.18 g/cm^3	~2.1 g/cm^3

Table 3: Physical properties of GO.

Diameter	Thickness	Single layer ratio	Purity
500 nm–5 μm	0.8–1.2 nm	~ 99%	> 99wt%

Where $P(r)$ is the cumulative mercury pressure, γ is the surface tension of mercury that equals to 358.2 dyn/cm, θ is the contact angle between solid surface and mercury that equals to 140° in this test.

Differentiating Eq. (6) with respect to r and $P(r)$, Eq. (7) can be written as:

$$P(r)\mathrm{d}r + r\mathrm{d}P(r) = 0 \tag{7}$$

Finally, combining of the Eqs. (5), (6) and (7), the fractal dimension D_M can be obtained through the following equation:

$$\lg\left[\frac{dV_{p(r)}}{dP(r)}\right] \propto (D_M - 4)\lg P(r) \tag{8}$$

Where, the fractal dimension D_M of the specimens can be obtained by calculating the slope of the double logarithmic regression fitting relationship between $P(r)$ and $\mathrm{d}V_{P(r)}/\mathrm{d}P(r)$.

3 Experimental process

3.1 Materials and instrumentation

In this study, graphene oxide-carbon nanotube based cementitious pastes were created using carbon nanomaterials as GO, MWCNTs (manufactured by Nanjing XFNANO Materials Tech Co, Nanjing City Jiangsu Province, China) and cement. Type P.O. 42.5 Portland cement, which satisfies the Chinese Standard GB175-2007 [31], was picked. The chemical composition and physical properties of commercially manufactured GO, MWCNTs and OPC are exhibited in Table 1, 2, and 3, respectively. One commercial polycarboxylate-based surfactant (PC) was picked to enhance the dispersion degree of the GO/MWCNTs in suspensions [24].

A horn ultrasonicator (VCX 500W) which can monitor the energy transferred to the suspensions in real time, with a cylindrical tip (end diameter: 13mm), was used for ultrasonication. The pore structures of the samples were characterized by mercury intrusion porosimeter (MIP) at ages of 28 days using AutoPore IV9500.

3.2 Preparation of specimens

A mixture containing five different components, as distilled water, GO, MWCNTs, PC and dry cement powder were first prepared. According to the author's previous studies [15, 32], the concentration of MWCNTs and GO were defined as 0.04 wt.% and 0.02 wt.% relative to the overall weight of the suspensions, while the PC-to-suspensions ratio was chosen as 0.48 wt.% (8 times the weight of the carbon nanomaterials). After stirring the materials for 5 mins, the solution then was ultrasonicated to create the GO/MWCNT suspensions. The whole ultrasonication process was under a pulse mode with a short 3-second-pause during every 6-second period. A water-ice bath was placed surrounding the suspensions during the ultrasonication process to prevent overheating. Two series of GO/MWCNT suspensions were created with power-controlled and time-controlled ultrasonication, respectively. For the power-controlled, the power levels of ultrasonication were set as 55, 64, 73, 81, 87, 94, 109 and 118W and the time lasted for 15 min of each sample. For the time-controlled series, the ultrasonication time was fixed at 1, 3, 5, 10. 15, 20, 30, 40, and 60 min with the 94 W amplitude.

After the dispersing of GO/MWCNTs in the solution, the suspensions then were added into the cement pow-

Table 4: Mercury intrusion porosimetry analysis of GO/MWCNT-OPC pastes.

Specimens	Ultrasonication			MIP results	
	Power (W)	Time (min)	UE (KJ)	Total intruded volume (ml/g)	Porosity(%)
P-1	–	–	–	0.175	29.6
A-1	55	15	24.8	0.167	26.9
A-2	64		28.8	0.157	26.1
A-3	73		32.9	0.142	24.5
A-4	81		36.5	0.134	23.2
A-5	87		39.2	0.127	22.2
A-6	94		42.3	0.136	23.8
A-7	109		49.1	0.148	25.1
A-8	118		53.1	0.162	26.8
B-1	94	1	2.82	0.164	27.8
B-2		3	8.46	0.149	25.2
B-3		5	14.1	0.153	25.5
B-4		10	28.2	0.149	25.4
B-5		15	42.3	0.147	24.8
B-6		20	56.4	0.137	23.5
B-7		30	84.6	0.138	24.0
B-8		40	112.8	0.134	23.1
B-9		60	169.2	0.133	23.1

(Note: UE represents the ultrasonication energy. P-1 represents the plain OPC pastes without any nano-additives.)

ders based on the 0.4 water-to-cement ratio (w/c). The fresh mixtures were stirred at moderate and high speed until the completion of mixing, and then the fresh pastes were poured into 20 mm × 40 mm × 160 mm molds with enough vibrated in order to remove the entrapped air and ensure compaction, after that the specimens were covered with wet films to prevent moisture escaping. The specimens were demolded after 24 hours and conserved in the saturated lime water at 20 ± 5°C for another 27 days before testing. Then the pore structures of GO/MWCNT-OPC harden pastes were characterized using MIP techniques and the fractal characteristics can be calculated. The detailed measurements of MIP tests are exhibited in Table 4 for GO/MWCNT-OPC pastes conducted by power- and time-controlled ultrasonication, respectively.

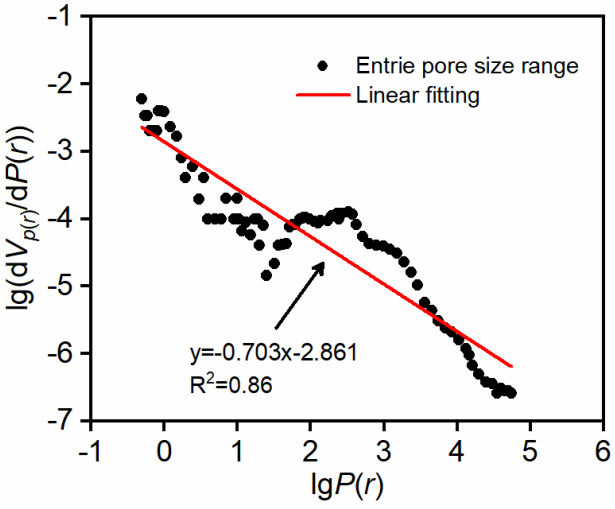

Figure 1: Logarithm plot of $\lg(dV_{P(r)}/dP(r))$ and $\lg P(r)$ in the entire pore size range (Sample P-1).

4 Results and discussion

4.1 Surface fractal characteristics in various pore-size ranges

Figure 1 presents the relation between $\lg\left[\frac{dV_{P(r)}}{dP(r)}\right]$ and $\lg P(r)$ fitting using the pore size distribution of the Sample P-1. According to the Eq. (8), the surface fractal dimension D_M can be obtained through the linear regression analysis based on the slope of the fitting line and the D_M is 3.297. According to the fractal theory [9], the fractal dimension ranges from 2 to 3 and $D_M = 2$ means that pore structure is extremely flat while $D_M = 3$ indicates that the pore characteristics become rough and irregular [33, 34]. In addition, a value of D_M more than 3 implies that the model is be-

Table 5: Mercury intrusion porosimetry analysis of GO/MWCNT-OPC pastes.

Specimens	Ultrasonication			Fractal dimensions		
	Power (W)	Time (min)	UE (KJ)	$D_{10-50nm}$	$D_{50-200nm}$	$D_{>10^4\ nm}$
P-1	–	–	–	2.706	2.741	2.733
A-1	55	15	24.8	2.874	2.582	2.761
A-2	64		28.8	2.755	2.477	2.87
A-3	73		32.9	2.694	2.629	2.888
A-4	81		36.5	2.614	2.462	2.843
A-5	87		39.2	2.209	2.334	2.965
A-6	94		42.3	2.622	2.353	2.839
A-7	109		49.1	2.577	2.796	2.728
A-8	118		53.1	2.805	2.318	2.673
B-1	94	1	2.82	2.914	2.380	2.772
B-2		3	8.46	2.874	2.582	2.761
B-3		5	14.1	2.804	2.320	2.792
B-4		10	28.2	2.814	2.720	2.814
B-5		15	42.3	2.711	2.530	2.834
B-6		20	56.4	2.729	2.771	2.902
B-7		30	84.6	2.628	2.683	2.887
B-8		40	112.8	2.545	2.924	2.870
B-9		60	169.2	2.228	2.236	2.954

yond the three-dimensional space concept, and thus, it should not be considered as a physical from the geometric perspective [9]. As exhibited in Figure 1, the D_M for the Sample P-1 is against the fundamental assumptions of fractal theory. In addition, as it can be seen, the coefficient of linear fitting of R^2 is only up to 0.86, indicating that it is not reasonable to analyze the fractal dimension of the pore size range as a whole. Moreover, the pore characteristics of the cement-based materials include various pore sizes, ranging from nanoscale gel pores entrapped among the calcium silicate hydrate (C-S-H) hydration products to milli scale inside air voids [35], which influences the properties of the cementitious materials, such as the mechanical strength, permeability, and durability. The fractal dimension obtained from the entire pore size distribution range may present limitations of the materials [36].

To better describe the variations of the fractal characteristics of the test samples, the contribution and fractal dimension of five different types of pores as mesopores, middle capillary pores, bigger capillary pores with sizes <10, 10-50, 50-200,200-10000, and >10000 nm were considered respectively [37]. Figure 2 exhibits the relations between $\lg\left[\frac{dV_{p(r)}}{dP(r)}\right]$ and $\lg P(r)$ for five regions of the test specimens, and the fractal dimensions are denoted as $D_{<10\,nm}$, $D_{10-50\,nm}$, $D_{50-200\,nm}$, $D_{200-10^4\,nm}$ and $D_{>10^4\,nm}$, respectively. However, the $D_{<10\,nm}$ and $D_{200-10^4\,nm}$ are not recorded due to conflict with the fundamental assumptions of fractal theory. The detailed measurements are presented in Table 4 in three regions.

As exhibited in Figure 2, Figure 3 and Table 4, the mesopores in the ranges of 10-50 nm and 50-200 nm and bigger capillary pores with diameters larger than 10^4 nm are presented the fractal dimensions. The fractal characteristics of the bigger capillary pores, corresponding to the pores which are full of hydration products [19], are from 2.673 to 2.965. While the fractal dimensions of the mesopores in the range of 10-50 nm and 50-200 nm are 2.209-2.914 and 2.236-2.924, respectively.

4.2 Impact of power- and time-controlled

The correlations between the power-/time-controlled ultrasonication energy (UE) and the fractal dimensions of three pore size ranges $D_{10-50\,nm}$, $D_{50-200\,nm}$, and $D_{>10^4\,nm}$ of the GO/MWCNT-OPC pastes are shown in Figure 4. As can be seen from Figure 4a, the $D_{10-50\,nm}$ started at 2.874, the value declines constantly as the increase of the ultrasonication power and hits the minimum at 2.209 (Sample A-5), after that the figure rises again with the increase of ultrasonic energy. The value of $D_{>10^4\,nm}$ shows an opposite trend, whose figure grow continuously with the increase of the ultrasonication power and hit the peak at Sample A-5 ($D_{>10^4\,nm} = 2.965$) too, after that the value shows a de-

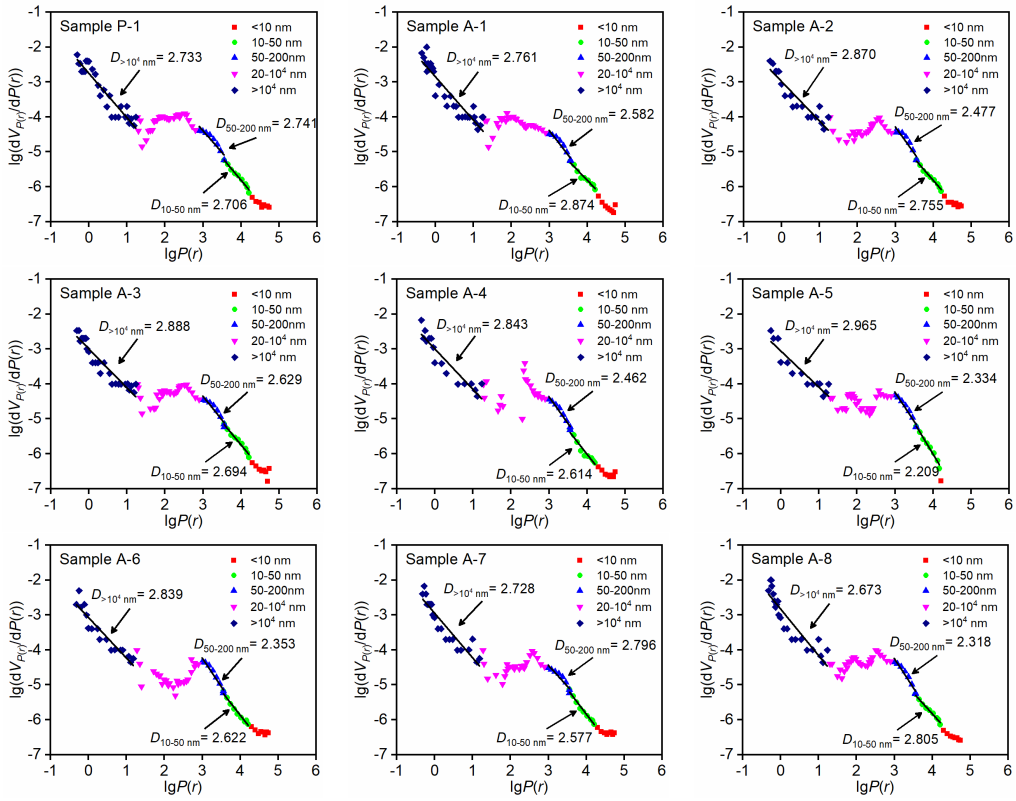

Figure 2: Logarithm plot of lg(d$V_{P(r)}$/d$P(r)$) and lg$P(r)$ in the different pore size range under power-controlled ultrasonication.

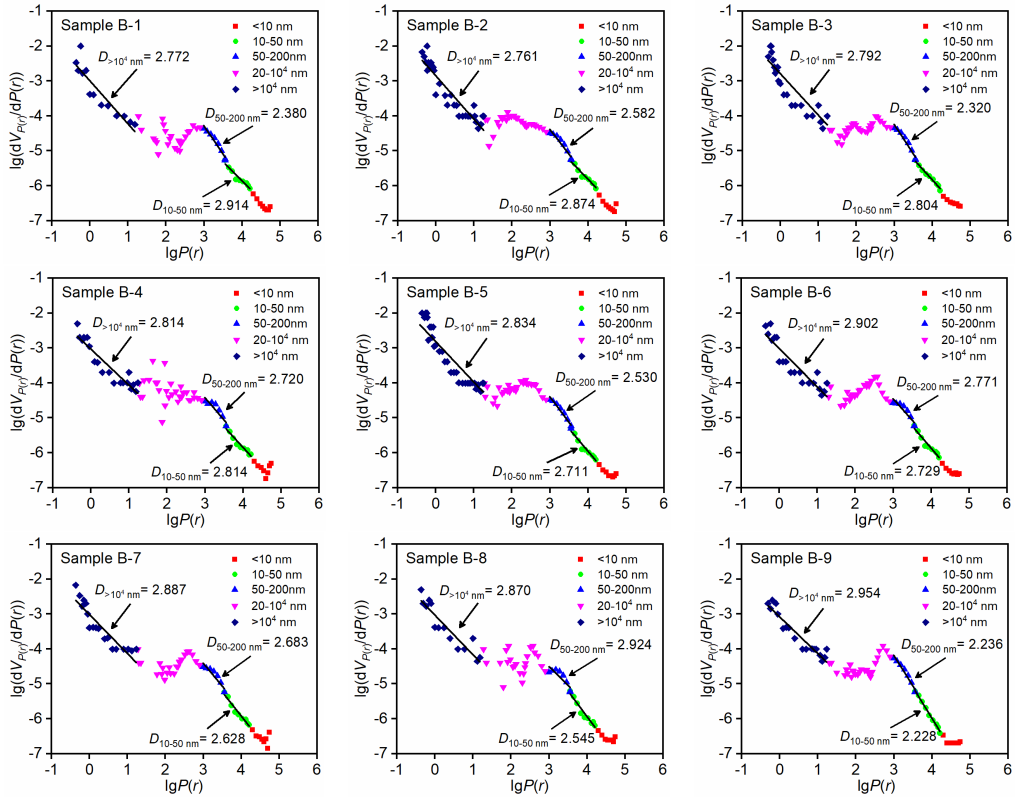

Figure 3: Logarithm plot of lg(d$V_{P(r)}$/d$P(r)$) and lg$P(r)$ in the different pore size range under time-controlled ultrasonication.

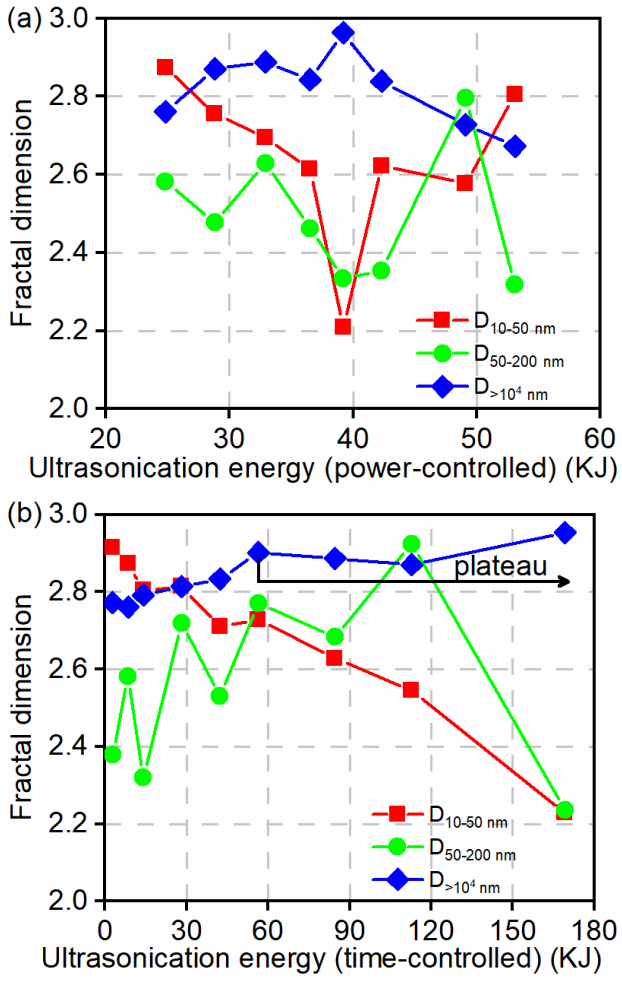

Figure 4: Effect of ultrasonication energy on the fractal dimensions of GO/MWCNT-OPC pastes: (a) power-controlled, (b) time-controlled.

clined trend. However, the figure of the $D_{50-200\,nm}$ shows a fluctuation state. According to the previous studies [15], in the power-controlled condition, with the increase of the ultrasonication energy, the degree of GO/MWCNTs materials dispersion enhanced constantly due to the ultrasonication separating forces while the length of the MWCNTs and the average diameter of the GO sheets were reduced respectively because of the ultrasonication scissoring forces. While the higher degree of dispersion and the well length distribution of the carbon nanomaterials contribute to a better pore structures of the cement-based pastes and higher fractal dimensions. Therefore, combined with the MIP test results, it implies that at the front of ultrasonication power growth, the ultrasonication separating forces play a major role, reinforcing the pore characteristics particularly in the bigger capillary pores. When the ultrasonication power continuously increases, the effects of the ultrasonication scissoring forces will exceed the separating forces and influence the pore structure of GO/MWCNT-OPC pastes. Moreover, the change trends of $D_{10-50\,nm}$ and $D_{>10^4\,nm}$ are always the opposite which indicates that a certain amount of GO/MWCNTs materials reinforce the larger pores at first under better ultrasonication conditions.

Figure 4b indicates the effects of the time-controlled ultrasonication on the fractal dimensions at three ranges $D_{10-50\,nm}$, $D_{50-200\,nm}$, and $D_{>10^4\,nm}$ of the GO/MWCNT-OPC pastes. With the increase of the ultrasonication time, the value of $D_{10-50\,nm}$ exhibits a downward trend constantly, while that of $D_{>10^4\,nm}$ shows an upward trend with a plateau when the ultrasonication time exceeds 60 KJ. This phenomenon implies that at relatively low power, increasing ultrasonication time may only influence the mesopores, reducing its fractal dimensions, while little cause the change of the ultrasonication scissoring forces and has less impact on macro pores. The findings are in good agreement with the previous studies that prolongation the ultrasonication time little affect the dispersion of GO/MWCNTs in the suspensions and the mechanical properties of its cement-based pastes. However, the further increase of the ultrasonication power may cause the deterioration of these items.

5 Conclusions

This study investigates the fractal dimensions of pore structures of GO/MWCNT-OPC pastes in power- and time-controlled ultrasonication. The main findings are as follow:

(1) The fractal dimension obtained from the overall pore size ranges presents limitations of the materials. To allow for better fractal analysis and evaluate the pore characteristics of specimens, it is more feasible to assess the variations of fractal dimension of the individual pore size range of the GO/MWCNT-OPC pastes, the contribution of five different types of pores as mesopores, middle capillary pores, bigger capillary pores with the sizes <10, 10-50, 50-200,200-10^4, and >10^4 nm.

(2) The correlation between the ultrasonication energy and mechanical properties, permeability, and durability of the GO/MWCNT-OPC pastes owns the similar change trend with the relationship between that and the fractal dimension of the bigger capillary pores ($D_{>10^4\,nm}$). Moreover, the change trends of $D_{10-50\,nm}$ and $D_{>10^4\,nm}$ with ultrasonication energy are always the opposite, indicating that a certain

amount of GO/MWCNTs materials could reinforce the larger pores at first under better ultrasonication treatment.

(3) The moderate increment of ultrasonication power and time may both enhance the pore structures of the GO/MWCNT-OPC pastes by increasing the factual dimension of bigger capillary pores ($D_{>10^4\ nm}$). After that, excess ultrasonication energy in power-controlled treatment would cause the deterioration of the pore structures, decreasing the capillary pores factual dimension, while prolonging the ultrasonication time has little influence on the pore structures.

It is expected that the results of this study could provide helpful information in the fields of analyzing and predicting the mechanical and transport properties of the carbon nanomaterials additive cementitious composites under different ultrasonication treatments.

Acknowledgement: This study was supported by the National Natural Science Foundation of China, China (No. 51734009) and Postgraduate Education Reform Project of Jiangsu Province, China.

Conflict of Interests: The authors declare no conflict of interest.

References

[1] T. Matusinović, J. Šipušić, N. Vrbos, Porosity-strength relation in calcium aluminate cement pastes, Cem. Concr. Res. (2003). doi:10.1016/S0008-8846(03)00201-1.

[2] A.U. Ozturk, B. Baradan, A comparison study of porosity and compressive strength mathematical models with image analysis, Comput. Mater. Sci. (2008). doi:10.1016/j.commatsci.2008.02.011.

[3] C. Atzeni, G. Pia, U. Sanna, A geometrical fractal model for the porosity and permeability of hydraulic cement pastes, Constr. Build. Mater. (2010). doi:10.1016/j.conbuildmat.2010.04.020.

[4] R. Liu, H. Xiao, H. Li, L. Sun, Z. Pi, G.Q. Waqar, T. Du, L. Yu, Effects of nano-SiO2 on the permeability-related properties of cement-based composites with different water/cement ratios, J. Mater. Sci. (2018). doi:10.1007/s10853-017-1906-8.

[5] C.W. Kilmister, B.B. Mandelbrot, Fractals: Form, Chance and Dimension, Math. Gaz. (2007). doi:10.2307/3617679.

[6] J.W. Cannon, B.B. Mandelbrot, The Fractal Geometry of Nature., Am. Math. Mon. (1984). doi:10.2307/2323761.

[7] Q. Zeng, K. Li, T. Fen-Chong, P. Dangla, Surface fractal analysis of pore structure of high-volume fly-ash cement pastes, Appl. Surf. Sci. (2010). doi:10.1016/j.apsusc.2010.07.061.

[8] Y. Wang, S. Diamond, A fractal study of the fracture surfaces of cement pastes and mortars using a stereoscopic SEM method, Cem. Concr. Res. (2001). doi:10.1016/S0008-8846(01)00591-9.

[9] B. Zhang, S. Li, Determination of the Surface Fractal Dimension for Porous Media by Mercury Porosimetry, Ind. Eng. Chem. Res. (1995). doi:10.1021/ie00043a044.

[10] B. Zhang, W. Liu, X. Liu, Scale-dependent nature of the surface fractal dimension for bi- and multi-disperse porous solids by mercury porosimetry, Appl. Surf. Sci. (2006). doi:10.1016/j.apsusc.2006.02.009.

[11] R. Blinc, G. Lahajnar, S. Umer, M.M. Pintar, NMR study of the time evolution of the fractal geometry of cement gels, Phys. Rev. B. (1988). doi:10.1103/PhysRevB.38.2873.

[12] D. Pearson, A.J. Allen, A study of ultrafine porosity in hydrated cements using small angle neutron scattering, J. Mater. Sci. (1985). doi:10.1007/BF00555924.

[13] H.M. Jennings, J.J. Thomas, J.S. Gevrenov, G. Constantinides, F.J. Ulm, A multi-technique investigation of the nanoporosity of cement paste, Cem. Concr. Res. (2007). doi:10.1016/j.cemconres.2006.03.021.

[14] H.M. Jennings, J.W. Bullard, J.J. Thomas, J.E. Andrade, J.J. Chen, G.W. Scherer, Characterization and Modeling of Pores and Surfaces in Cement Paste: Correlations to Processing and Properties, J. Adv. Concr. Technol. (2008). doi:10.3151/jact.6.5.

[15] Y. Gao, H.W. Jing, S.J. Chen, M.R. Du, W.Q. Chen, W.H. Duan, Influence of ultrasonication on the dispersion and enhancing effect of graphene oxide–carbon nanotube hybrid nanoreinforcement in cementitious composite, Compos. Part B Eng. (2019). doi:10.1016/j.compositesb.2018.11.066.

[16] F. Collins, J. Lambert, W.H. Duan, The influences of admixtures on the dispersion, workability, and strength of carbon nanotube-OPC paste mixtures, Cem. Concr. Compos. (2012). doi:10.1016/j.cemconcomp.2011.09.013.

[17] A.K. Geim, K.S. Novoselov, The rise of graphene, Nat. Mater. (2007). doi:10.1038/nmat1849.

[18] Z. Dai, W. Chen, G. Lv, W. Hu, D. Li, S. Chen, Synthesis and applications of graphene quantum dots: a review, Nanotechnol. Rev. 7 (2018) 157–185. doi:10.1515/ntrev-2017-0199.

[19] D. Hou, Z. Lu, X. Li, H. Ma, Z. Li, Reactive molecular dynamics and experimental study of graphene-cement composites: Structure, dynamics and reinforcement mechanisms, Carbon N. Y. (2017). doi:10.1016/j.carbon.2017.01.013.

[20] K. Gong, S.M. Asce, Z. Pan, A.H. Korayem, D. Ph, L. Qiu, D. Li, F. Collins, C.M. Wang, W.H. Duan, a M. Asce, Reinforcing Effects of Graphene Oxide on Portland Cement Paste, J. Mater. Civ. Eng. (2014). doi:10.1061/(ASCE)MT.1943-5533.0001125.

[21] C. Zhang, L. Ren, X. Wang, T. Liu, Graphene oxide-assisted dispersion of pristine multiwalled carbon nanotubes in aqueous media, J. Phys. Chem. C. (2010). doi:10.1021/jp103745g.

[22] C. Zhou, F. Li, J. Hu, M. Ren, J. Wei, Q. Yu, Enhanced mechanical properties of cement paste by hybrid graphene oxide/carbon nanotubes, Constr. Build. Mater. (2017). doi:10.1016/j.conbuildmat.2016.12.147.

[23] Y. Gao, H.W. Jing, Z.F. Zhou, W.Q. Chen, M.R. Du, Y. Du, Influence of graphene oxide-carbon nanotube hybrid nano-reinforcement on the transport properties of cementitious composites with different water-to-cement ratios, Constr. Build. Mater.

[24] B. Zou, S.J. Chen, A.H. Korayem, F. Collins, C.M. Wang, W.H. Duan, Effect of ultrasonication energy on engineering properties of carbon nanotube reinforced cement pastes, Carbon N. Y. (2015). doi:10.1016/j.carbon.2014.12.094.

[25] S.J. Chen, B. Zou, F. Collins, X.L. Zhao, M. Majumber, W.H. Duan, Predicting the influence of ultrasonication energy on the reinforcing efficiency of carbon nanotubes, Carbon N. Y. 77 (2014) 1–10. doi:10.1016/j.carbon.2014.04.023.

[26] A. Lucas, C. Zakri, M. Maugey, M. Pasquali, P. Van Der Schoot, P. Poulin, Kinetics of nanotube and microfiber scission under sonication, J. Phys. Chem. C. (2009). doi:10.1021/jp906296y.

[27] M.S. Strano, V.C. Moore, M.K. Miller, M.J. Allen, E.H. Haroz, C. Kittrell, R.H. Hauge, R.E. Smalley, The Role of Surfactant Adsorption during Ultrasonication in the Dispersion of Single-Walled Carbon Nanotubes, J. Nanosci. Nanotechnol. 3 (2003) 81–86. doi:10.1166/jnn.2003.194.

[28] E. Perfect, B.D. Kay, Applications of fractals in soil and tillage research: a review, Soil Tillage Res. (1995). doi:10.1016/0167-1987(96)81397-3.

[29] D. Giménez, E. Perfect, W.J. Rawls, Y. Pachepsky, Fractal models for predicting soil hydraulic properties: a review, Eng. Geol. (2002). doi:10.1016/s0013-7952(97)00038-0.

[30] L.R. Fisher, P.D. Lark, An experimental study of the washburn equation for liquid flow in very fine capillaries, J. Colloid Interface Sci. (1979). doi:10.1016/0021-9797(79)90138-3.

[31] C.S. GB175, Common portland cement, Beijing, PR China. (2007).

[32] Y. Gao, H. Jing, M. Du, W. Chen, Dispersion of Multi-Walled Carbon Nanotubes Stabilized by Humic Acid in Sustainable Cement Composites, (2018). doi:10.3390/nano8100858.

[33] M.M. Mahamud, J.M. Menéndez, P.E. Sarquís, CO2 activation of chars: Effect of burn-off on texture and fractal properties, Fuel Process. Technol. (2014). doi:10.1016/j.fuproc.2013.10.009.

[34] G.J. Lee, S. Il Pyun, The effect of pore structures on fractal characteristics of meso/macroporous carbons synthesised using silica template [8], Carbon N. Y. (2005). doi:10.1016/j.carbon.2005.02.009.

[35] P.K. Mehta, P.J.M. Monteiro, Concreto: Microestrutura, Propriedades e Materiais., 2014. doi:10.1036/0071462899.

[36] J. Kim, Y.C. Choi, S. Choi, Fractal Characteristics of Pore Structures in GGBFS-based Cement Pastes, Appl. Surf. Sci. (2018). doi:10.1016/j.apsusc.2017.09.165.

[37] Y. Zhao, Z. Feng, Y. Zhao, Z. Wan, Experimental investigation on thermal cracking, permeability under HTHP and application for geothermal mining of HDR, Energy. (2017). doi:10.1016/j.energy.2017.05.093.